Heat and Mass Transfer 31 (1996) 269–277 © Springer-Verlag 1996

Analytical solutions for laminar fully developed flows in double-sine shaped ducts

J. Ding, R. M. Manglik

Abstract Fully developed, constant property, laminar flows in double-sine shaped ducts are considered. This cross section represents a limiting inter-plate channel geometry in plate heat exchangers. Accurate analytical solutions based on the Galerkin integral method are presented. Heat transfer with both T and H1 thermal boundary conditions is analyzed; they simulate the most fundamental practical heating/cooling applications. Velocity and temperature distributions, along with fRe, Nu_T, and Nu_{H1} results for flows in double-sine ducts of different aspect ratios ($1/8 \leq \gamma \leq 8$) are presented. Effects of the relative cross-sectional geometry and thermal boundary conditions are delineated. A comparison of the thermal-hydraulic performance with that of other compact channel geometries is made. The results suggest an optimum (Nu/fRe) performance in a double-sine duct of aspect ratio near unity.

Analytische Lösungen für vollausgebildete Laminarströmungen in zweiseitig sinusförmig ausgebildeten Kanälen

Zusammenfassung Es werden vollausgebildete Laminarströmungen in zweiseitig sinusförmig ausgebildeten Kanälen unter Voraussetzung konstanter Stoffwerte untersucht. Der Querschnitt repräsentiert die geschachtelte Trennwandanordunung von Plattenwärmetauschern. Exakte Lösungen, gewonnen mittels der Galerkinschen Integralmethode, werden mitgeteilt, wobei für den Wärmeübergang die thermischen Randbedingungen $T=$ const. und $\dot{q}=$ const. zugrunde liegen, welche die wichtigsten praktischen Anwendungsfälle bei Heizung oder Kühlung simulieren. Die Darstellung der Ergebnisse umfaßt die Geschwindigkeits- und Temperaturfelder, die Reibungsbeiwerte und Nusselt-Zahlen im Bereich des Seitenverhältnisses $1/8 \leq \gamma \leq 8$. Die Einflüsse der bezogenen Kanalquerschnittsgeometrie und der thermischen Randbedingungen werden dargelegt. Ferner erfolgt ein Vergleich des thermisch-hydraulischen Verhaltens mit jenem für andere Kanalgeometrien von Kompaktwärmetauschern. Die Ergebnisse lassen erkennen, daß für doppelseitig sinusförmig ausgebildete Kanäle optimales Übertragungsverhalten bei einem Seitenverhältnis nahe Eins resultiert.

Received on 16 May 1995

J. Ding
R. M. Manglik
Department of Mechanical, Industrial and Nuclear Engineering
University of Cincinnati
Cincinnati, OH 45221-0072, USA

Correspondence to: R. M. Manglik

This study was supported by The Procter & Gamble Co., Cincinnati, OH, USA, and the Thermal-Fluids Laboratory, University of Cincinnati, Cincinnati, OH, USA.

Nomenclature

a, b	characteristic dimensions of the duct, Fig. 2
a_k, b_k, c_k	coefficients of series solution, Eq. (18)
A_c	duct cross-sectional area (m2)
c_p	specific heat of fluid at constant pressure (J/kg K)
d_h	hydraulic diameter, $4A_c/P_w$ (m)
d_n	eigenvector corresponding to the nth eigenvalue, Eq. (22)
f	Fanning friction factor, Eq. (26)
H1	constant wall heat flux with uniform peripheral temperature boundary condition
h	convective heat transfer coefficient (W/m2 K)
k	fluid thermal conductivity (W/m K)
Nu	peripherally average Nusselt number, hd_h/k
p	fluid pressure (N/m2)
P_w	wetted perimeter (m)
Pr	fluid Prandtl number, $\mu c_p/k$
Re	Reynolds number, $\rho u_m d_h/\mu$
T	temperature (K)
T	constant wall temperature boundary condition
u, u_m	axial and axial mean velocity (m/s)
U, U^*, U_m	dimensionless axial velocity, Eqs. (5), (21) and (26)
x, y, z	cartesian coordinates (m)
X, Y	dimensionless cartesian coordinates, Eq. (4)

Greek symbols

α	thermal diffusivity, $k/\rho c_p$
γ	aspect ratio of the duct cross section, $2b/2a$
Γ_y, Γ_Y	dimensional and non-dimensional contour of duct cross-section, Eqs. (1) and (12)
θ	dimensionless temperature, Eq. (6)
λ_n	the nth eigenvalue, Eqs. (24) and (25)
μ	fluid dynamic viscosity (N s/m2)
ρ	fluid density (kg/m2)
ψ	Galerkin function, Eqs. (14) and (18)
ω	weight function, Eq. (17)

Subscripts

b	bulk or mixing-cup value
$H1$	pertaining to the H1 thermal boundary condition
m	mean value
max	maximum value
T	pertaining to the T thermal boundary condition
w	at the duct wall

1 Introduction

Laminar flow heat transfer in complex duct geometries is of both fundamental and practical interest. Analytical, numerical and experimental results for such flows are essential for the design and application of compact heat exchangers. In the use of compact surfaces and/or heat transfer enhancement devices, many different irregular and non-circular duct shapes are obtained [1–3]. Of particular interest is the plate heat exchanger, which has found an increasingly wide spectrum of applications in food and chemical processing, heat recovery, and refrigeration, among others [4, 5], in recent years. It consists of corrugated plates that are gasketed and stacked together within a bolted frame, in a manner that provides two-fluid stream flow passages in alternate inter-plate channels (additional constructional details are given in Refs. [4, 5]). There are more than 60 different plate surface corrugation patterns [4], and some typical corrugation profiles and the corresponding channel geometries are illustrated in Fig. 1. These modifications essentially provide for larger surface area and small hydraulic diameter channels, thereby promoting enhanced heat transfer.

Several investigations have reported solutions for laminar flow and heat transfer in circular and non-circular ducts [1, 6], and this problem continues to evoke much research interest [7–9]. Of the different duct shapes shown in Fig. 1, Shah [10] has reported analytical solutions for fully developed laminar flows in triangular, sine, rhombic, and trapezoidal ducts. In all these cases, isothermal friction factor and Nusselt number results for the H1 and H2 thermal boundary conditions are presented. Schmidt and Newell [11] and Haji-Sheikh et al. [12] have considered the T boundary conditions for triangular and rectangular ducts. Additionally, for the T boundary condition, heat transfer results for a rhombic duct are given by Asako and Faghri [13], for a trapezoidal duct by Farhanieh and Sunden [8], and for sine shaped channels by Sherony and Solbrig [14].

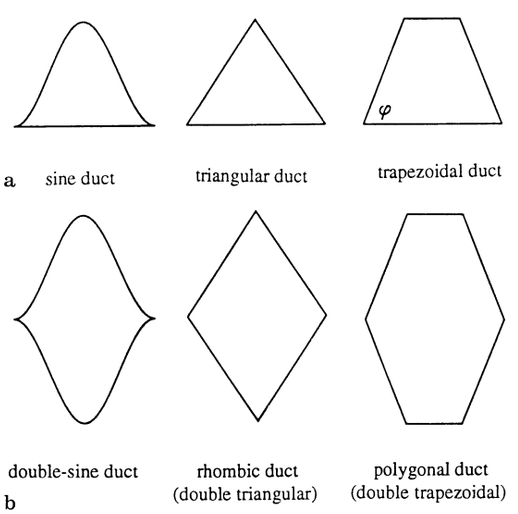

Fig. 1a, b. Typical channel geometries employed in corrugated plate heat exchangers. a basic shape, b channel contours obtained in plate-and frame heat exchangers

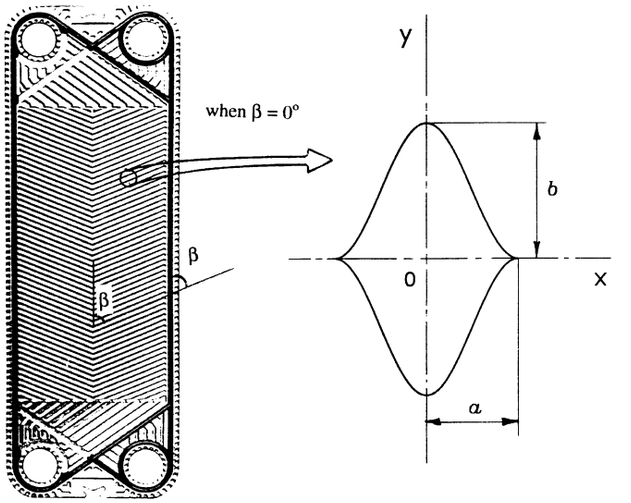

Fig. 2. Flow cross-section geometry and coordinate system for a double-sine shaped duct in chevron plate ($\beta = 0^\circ$) passages

A valuable collection of heat transfer and pressure drop results for laminar flows in a variety of different channel shapes is given in Refs. [1, 6].

The more widely used plate heat exchangers consist of plates with chevron type corrugations that have a sinusoidal shape [4], as shown in Fig. 2. When the chevron inclination angle $\beta = 0^\circ$ for these corrugations, the inter-plate flow channels have a double-sine shaped cross section. In effect, laminar flow heat transfer in a double-sine duct represents a limiting case for the heat transfer enhancement due to chevron plates. However, despite their increased usage over the last several decades for many different applications [4, 5], results for such flows do not appear to have been reported in the literature. This is addressed in the present study, and velocity and temperature field solutions for hydrodynamically and thermally fully developed laminar flow are presented. For the heat transfer problem, both the constant wall temperature (T) and constant wall heat flux with peripherally constant temperature (H1) boundary conditions are considered.

A large body of the heat transfer literature has dealt with numerical and analytical solutions for duct flow problems [1, 6]. Often, due to the complex channel cross-section geometry, closed form analytical solutions are difficult to attain. A particularly powerful and quite accurate technique, that readily lends to solutions for irregular shaped duct flows, is the Galerkin integral method [12, 15, 16]. Haji-Sheikh et al. [12] and Lakshminarayanan and Haji-Sheikh [7], among others [17–19], have demonstrated the effectiveness of this technique. Very accurate results for laminar flows in triangular and rectangular ducts, for both thermal entrance region and fully developed conditions, have been presented [7, 12, 17]. In the present study also, the Galerkin integral method has been employed to obtain solutions for fully developed laminar flows in double-sine shaped ducts. As explained earlier, these results have much significance in the practical usage of, and evaluation of the heat transfer enhancement in plate heat exchangers with sinusoidally corrugated plates.

2 Mathematical analysis

Many fundamental problems in mechanics, that are governed by differential equations and the so-called minimum principles, can be solved by determining the equilibrium position corresponding to the minimum potential energy of the given mechanical system. This is essentially the mathematical basis of the Galerkin's integral method [15], i.e. to obtain the solution by minimizing the integral of the governing differential equation that describes the specified problem. This method is applied in the present study to obtain solutions for the velocity and temperature fields in fully developed laminar flows with heat transfer in straight ducts of double-sine shaped cross sections.

The geometrical details and the variables that describe the relevant attributes of a double-sine duct are shown in Fig. 2. The outer boundary or the contour of the duct is described by

$$\Gamma_y = \pm b\cos(\pi x/2a), \quad -a \le x \le a, \ -b \le y \le b \tag{1}$$

Steady state, constant property, hydrodynamically and thermally fully developed laminar flow is considered. Also, axial conduction and viscous dissipation are ignored; these are reasonable idealizations for most large *Pe* and *Pr* flows [1, 6, 9]. The corresponding axial momentum and energy conservation equations can be expressed as

$$\mu\left(\frac{\partial^2 u}{\partial x^2}+\frac{\partial^2 u}{\partial y^2}\right)=\frac{\partial p}{\partial z} \tag{2}$$

$$k\left(\frac{\partial^2 T}{\partial x^2}+\frac{\partial^2 T}{\partial y^2}\right)=\rho c_p u\frac{\partial T}{\partial z} \tag{3}$$

where, for thermally fully developed flows,

$$\frac{\partial T}{\partial z}=\begin{cases}[(T_w-T)/(T_w-T_b)]\,(\mathrm{d}T_b/\mathrm{d}z) & \text{for T}\\ (\mathrm{d}T_b/\mathrm{d}z) & \text{for H1}\end{cases}$$

Equations (2) and (3) are subject to the following boundary conditions:

$$u=0, \quad T=T_w \quad \text{on } \Gamma$$

In order to render the governing differential equations dimensionless, the following variables, that represent the dimensionless space coordinates, axial velocity, and fluid temperature, are introduced:

$$X=(x/2a), \quad Y=(y/2a) \tag{4}$$

$$U=u/[(4a^2/\mu)\,(\mathrm{d}p/\mathrm{d}z)], \quad U^*=u/u_m \tag{5}$$

$$\theta=(T_w-T)/[(4a^2 u_m/\alpha)\,(\mathrm{d}T_b/\mathrm{d}z)],$$

$$\theta_b=(T_w-T_b)/[(4a^2 u_m/\alpha)\,(\mathrm{d}T_b/\mathrm{d}z)] \tag{6}$$

where u_m is the average axial flow velocity and T_b is the bulk mean temperature. These are given by their usual definitions, respectively, as

$$u_m=\frac{1}{A_c}\int_{A_c} u\,\mathrm{d}A_c \tag{7}$$

$$T_b=\frac{1}{u_m A_c}\int_{A_c} uT\,\mathrm{d}A_c \tag{8}$$

With the substitution of the dimensionless variables, Eqs. (2) and (3) can be rewritten as

$$\frac{\partial^2 U}{\partial X^2}+\frac{\partial^2 U}{\partial Y^2}-1=0 \tag{9}$$

$$\frac{\partial^2 \theta}{\partial X^2}+\frac{\partial^2 \theta}{\partial Y^2}-\Theta=0 \tag{10a}$$

where

$$\Theta=\begin{cases}-U^*\theta/\theta_b & \text{for T}\\ -U^* & \text{for H1}\end{cases} \tag{10b}$$

which are subject to the following boundary conditions:

$$U=0, \quad \theta=0 \quad \text{on } \Gamma \tag{11a}$$

$$U, \theta \text{ are finite at } X=Y=0 \tag{11b}$$

Note that the dimensionless representation of the contour of the duct geometry given by Eq. (1) can be expressed as

$$\Gamma_Y=\pm\frac{\gamma}{2}\cos(\pi X), \quad -\tfrac{1}{2}\le X\le\tfrac{1}{2}, \quad -\frac{\gamma}{2}\le Y\le\frac{\gamma}{2} \tag{12}$$

where $\gamma=2b/2a$ is the aspect ratio of the double-sine duct cross section.

The application of the Galerkin integral method and the Euler–Lagrange equation problem requires that solutions for Poisson-type governing differential equations correspond to the minimum of the integral

$$I=\int\int_{A_c}[\,\nabla^2\Phi(X,Y)+2f(X,Y)\Phi]\,\mathrm{d}X\,\mathrm{d}Y \tag{13}$$

over the duct cross section bounded by the shape contour Γ. According to the Galerkin procedure, the dependent variable can be functionally represented as

$$\Phi=\sum_{k=1}^{n} G_k\Psi_k(X,Y) \tag{14}$$

which unconditionally satisfies the boundary condition $\Phi=0$ on Γ. Consequently, the minimum value problem of Eq. (13) is equivalent to the solution of

$$\int\int_{A_c}[\,\nabla^2\Phi-f(X,Y)]\,\Psi_i\,\mathrm{d}X\,\mathrm{d}Y=0 \tag{15}$$

which gives the system of equations that define the coefficients G_k.

Note that in Eqs. (13) and (15) the function $f(X, Y)$ represents the following:

$$f(X,Y)=\begin{cases}1, & \Phi=U\\ -U^*\theta/\theta_b, & \Phi=\theta_T\\ -U^*, & \Phi=\theta_{H1}\end{cases} \tag{16}$$

Furthermore, the Galerkin function Ψ is described by X, Y and a weight function $\omega(X, Y)$, which in turn depends upon the duct flow geometry. Note that $\omega(X, Y)=0$ on the duct boundary, and for the double-sine shaped geometry (Fig. 2) it is given by

$$\omega(X,Y)=(Y+\tfrac{1}{2}\gamma\cos\pi X)\,(Y-\tfrac{1}{2}\gamma\cos\pi X) \tag{17}$$

Thus, the velocity and temperature field solutions given by Eq. (14) may be expressed as

$$\Phi = G_1\Psi_1 + G_2\Psi_2 + G_3\Psi_3 + \cdots + G_n\Psi_n$$
$$= \omega(X, Y)(G_1 + G_2X^2 + G_3Y^2 + G_4X^4 + G_5X^2Y^2 + G_6Y^4 + \cdots) \quad (18)$$

Here G_k can be designated as a_k, b_k, and c_k, respectively, corresponding to the field variables $\Phi = U, \theta_T$, and θ_{H1}, i.e.

$$U = \omega(X, Y)(a_1 + a_2X^2 + a_3Y^2 + a_4X^4 + a_5X^2Y^2 + a_6Y^4 + \cdots) \quad (18a)$$

$$\theta_T = \omega(X, Y)(b_1 + b_2X^2 + b_3Y^2 + b_4X^4 + b_5X^2Y^2 + b_6Y^4 + \cdots) \quad (18b)$$

$$\theta_{H1} = \omega(X, Y)(c_1 + c_2X^2 + c_3Y^2 + c_4X^4 + c_5X^2Y^2 + c_6Y^4 + \cdots) \quad (18c)$$

By substituting Eq. (18) in Eq. (15) and solving the resulting system of equations, the coefficients G_k (or a_k, b_k, and c_k) can be evaluated. This is quite straightforward for the U and θ_{H1} problems. For the velocity problem, the system of equations are

$$\sum_{k=1}^{n} a_k \int\int_{A_c} \left(\frac{\partial^2\Psi_k}{\partial X^2} + \frac{\partial^2\Psi_k}{\partial Y^2} \right) \Psi_i \, dX \, dY = \int\int_{A_c} \Psi_i \, dX \, dY \quad (19)$$

and for the temperature problem with H1 condition

$$\sum_{k=1}^{n} c_k \int\int_{A_c} \left(\frac{\partial^2\Psi_k}{\partial X^2} + \frac{\partial^2\Psi_k}{\partial Y^2} \right) \Psi_i \, dX \, dY = -\int\int_{A_c} \Psi_i U^* \, dX \, dY \quad (20)$$

In the latter case, $U^*(X, Y)$ is obtained from the velocity field solution as

$$U^* = (u/u_m) = \left[A_c \sum_{k=1}^{n} a_k \Psi_k(X, Y) \right] \Bigg/ \left[\int\int_{A_c} \sum_{k=1}^{n} a_k \Psi_k(X, Y) \, dX \, dY \right] \quad (21a)$$

Also, the maximum velocity occurs at the center of the axisymmetric duct cross section and

$$U^*_{max} = (u_{max}/u_m) = U^*(0, 0) \quad (21b)$$

For the temperature problem with the T boundary condition, however, combining Eqs. (15) and (18b) yields

$$\sum_{k=1}^{n} b_k \int\int_{A_c} \Psi_i \nabla^2 \Psi_k \, dX \, dY + \sum_{k=1}^{n} (b_k/\theta_b) \int\int_{A_c} U^* \Psi_i \Psi_k \, dX \, dY = 0 \quad (22)$$

This is an eigenvalue problem, and Eq. (22) can be restated in matrix form as

$$[\hat{A}]\{B\} + [\hat{C}]\{B'\} = 0 \quad (23)$$

where the elements $b'_k = (b_k/\theta_b)$. The solution of this equation takes the form

$$\{B\} = b_1\{d_1\}e^{\lambda_1 z} + b_2\{d_2\}e^{\lambda_2 z} + \cdots + b_n\{d_n\}e^{\lambda_n z} \quad (24)$$

where λ_n's are the eigenvalues that are obtained by solving

$$\det|\hat{A} + \lambda\hat{C}| = 0 \quad (25)$$

Equation (25) suggests that the eigenvalues λ_n are all negative if the matrix $[\hat{C}]$ is finite and positive; $\{d_n\}$ in Eq. (24) are the corresponding eigenvectors. Also, elements of the coefficients in Eq. (23) are obtained from

$$\hat{a}_{ik} = \int\int_{A_c} \Psi_i \nabla^2 \Psi_k \, dX \, dY \quad \text{and} \quad \hat{c}_{ik} = \int\int_{A_c} U^* \Psi_i \Psi_k \, dX \, dY$$

Having determined the velocity and temperature distributions, the corresponding fully developed friction factor and Nusselt number need to be calculated. From its definition and a force balance across an element of duct cross section, the Fanning friction factor is given by

$$fRe = -[(d_h/2a)^2]/(2U_m) = -[A_c(d_h/2a)^2] \Big/ \left(2\int\int_{A_c} U(X, Y) \, dX \, dY \right) \quad (26)$$

For the peripherally averaged Nusselt number, the usual hydraulic diameter based definition is employed. In the case of the H1 boundary condition, this is obtained from

$$Nu_{H1} = [(d_h/2a)^2]/(4\theta_b) \quad (27)$$

In the case of fully developed flow ($z \to \infty$) with the T boundary condition, it can be shown that the contribution of all eigenvalues, except λ_1, diminishes. Consequently, the Nusselt number can be calculated as

$$Nu_T = -\tfrac{1}{4}\lambda_1(d_h/2a)^2 \quad (28)$$

With the numerical computations of a_k, b_k, c_k, and λ_k, the velocity and temperature distributions, and isothermal friction factors and Nusselt numbers can be evaluated from Eqs. (18) and (26)–(28) for different aspect ratios of the duct cross section. These were carried out by using standard numerical techniques. The solutions of the linear simultaneous equations for coefficients a_k, b_k, and c_k were obtained by the Gauss–Jordan method [20]. The generalized eigenvalue problem in the temperature solution for the T condition was solved by Matlab version 4.2c.1 [21]. The numerical integration for one-dimensional and two-dimensional space domains, respectively, were executed by using Romberg and 16-point Gauss–Legendre algorithms [20]. The number of terms and coefficients in the series expansion were selected such that the maximum error was less than 0.01%, relative to the solution with larger number of terms; the friction factor, Nusselt number and peak values of velocity and temperature profiles attain virtually constant values as n increases, thereby indicating convergent solutions. Additional details of the analysis and solution methodology are given in Ref. [21].

In order to verify the reliability and accuracy of the above procedures, the problem of fully developed laminar flow with heat transfer in sine ducts was first solved. For this geometry, as mentioned earlier, Shah [10] has given analytical solutions for (u_{max}/u_m), fRe, and Nu_{H1}; Sherony and Solbrig [14] have given finite difference solutions for Nu_T. The comparison of the present results with those of Shah [10] and Sherony and Solbrig [14] is given in Table 1. As is evident from the tabulation, these results are in excellent agreement with those of previous studies, particularly with the analytical results of Ref. [10]. In the case of the T problem, the present solutions appear to be more accurate than those in Ref. [14].

Table 1. Fully developed laminar flow and heat transfer characteristics in sine ducts

$\gamma=\frac{2b}{2a}$	u_{max}/u_m		fRe		Nu_T		Nu_{H_1}	
	Present study	Ref. [10]	Present study	Ref. [10]	Present study	Ref. [14]	Present study	Ref. [10]
0	—	2.400	—	9.600	—	1.178*	—	1.920
1/8	2.357	2.357	9.7428	9.743	1.454	—	2.017	2.017
1/4	2.291	2.291	10.123	10.123	1.730	1.800	2.213	2.213
1/2	2.211	2.211	11.207	11.207	2.110	2.120	2.617	2.617
3/4	2.190	2.190	12.234	12.234	2.353	2.330	2.916	2.916
1.0	2.197	2.197	13.023	13.023	2.472	2.450	3.102	3.120
3/2	2.239	2.239	14.023	14.022	2.545	2.600	3.267	3.267
2.0	2.284	2.288	14.575	14.553	2.515	—	3.292	3.311
4.0	2.451	—	15.340	—	2.276	—	3.230	—
8	2.780	—	15.719	—	1.967	—	2.992	—
∞	—	3.825	—	15.303	—	0.739*	—	2.521

*Given in Refs. [1, 10]

3 Results and discussion

Analytical solutions for fully developed laminar flow with heat transfer in double-sine shaped ducts of different aspect ratios, $1/8 \leq \gamma \leq 8$, are presented. Both local (velocity and temperature distributions) and global (friction factor and Nusselt number) results are given, and the effects of ducts geometry and thermal boundary conditions (T and H1) on the performance are discussed.

3.1 Velocity and temperature fields

The velocity, U, and temperature, θ_T and θ_{H1}, distributions are given by Eqs. (18a)–(18c), respectively. The corresponding coefficients a_k, b_k, and c_k for different aspect ratio ducts are listed in Tables 2–4. It may be noted that more number of terms are needed in the series expansion of Eq. (18) as γ increases in order to obtain accurate solutions. For example, in Table 2 for the U distribution, 4 terms are needed for $\gamma=1/8$ and 21 terms for $\gamma=8$; similarly, as seen in Table 3, 6 terms are needed for θ_T solution with $\gamma=1/2$ and 21 terms are needed with $\gamma=4$ and 8. As mentioned previously, the numerical accuracy in all cases was ensured by successively increasing the number of terms in the series until the relative error was less than 0.01%.

The normalized velocity profiles, u/u_m, for three different aspect ratio ducts, $\gamma=0.25$, 1.0, and 4.0, are presented in Fig. 3. As can be seen, the duct aspect ratio greatly affects the velocity

Table 2. Coefficients a_k for the velocity distribution in double-sine ducts of different aspect ratio

a_k	$\gamma=2b/2a$						
	1/8	1/4	1/2	1.0	2.0	4.0	8.0
a_1	0.4823E+00	0.4412E+00	0.3443E+00	0.1968E+00	0.7867E−01	0.2466E−01	0.6846E−02
a_2	0.2978E+00	0.7361E+00	1.0003E+00	0.9571E+00	0.3665E+00	0.1199E+00	0.4151E−01
a_3	−0.4230E−01	−0.1174E+00	−0.1697E+00	−0.1362E+00	−0.5090E−01	−0.9584E−02	−0.1288E−02
a_4	−0.5655E+00	−0.1370E+00	3.7921E+00	0.1169E−01	3.5089E+00	1.2309E+00	−0.7374E−01
a_5		−0.0903E+00	−2.7011E+00	−1.7164E+00	−0.7439E+00	−0.1081E+00	−0.1244E−01
a_6		0.4582E−02	0.1703E+00	0.1428E+00	0.5014E−01	0.4754E−02	0.3363E−03
a_7				3.4449E+01	−2.4843E+01	−8.9684E+00	5.8846E+00
a_8				−2.6632E+01	−2.7607E+00	−0.3739E+00	−0.9533E−01
a_9				6.2056E+00	1.1778E+00	0.5843E−01	0.3547E−02
a_{10}				−0.2033E+00	−0.4451E−01	−0.1411E−02	−0.5196E−04
a_{11}					1.7112E+02	6.0947E+01	−4.6582E+01
a_{12}					−6.3486E+01	−6.5084E+00	0.1545E+00
a_{13}					1.1941E+01	0.3804E+00	0.1719E−01
a_{14}					−1.0880E+00	−0.1355E−01	−0.4582E−03
a_{15}					0.2011E−01	0.1671E−03	0.3897E−05
a_{16}							1.6841E+02
a_{17}							−6.4051E+00
a_{18}							0.1758E+00
a_{19}							−0.2513E−02
a_{20}							0.2280E−04
a_{21}							−0.1099E−06

Table 3. Coefficients b_k for the temperature distribution in double-sine ducts with the T boundary condition

b_k	$\gamma = 2b/2a$						
	1/8	1/4	1/2	1.0	2.0	4.0	8.0
b_1	1.0000E+00	1.0000E+00	1.0000E+00	1.0000E+00	1.0000E+00	1.0000E+00	1.0000E+00
b_2	−2.2427E+01	−1.4691E+01	−5.1581E+00	0.8355E−01	1.7662E+00	2.7694E+00	4.2462E+00
b_3	−1.0613E+02	−3.0224E+01	−1.0219E+01	−4.9411E+00	−3.0321E+00	−1.6581E+00	−0.8431E+00
b_4	1.1008E+02	5.7139E+01	1.1138E+01	4.6830E+00	2.9593E+01	3.0946E+01	−1.6410E+01
b_5	1.4979E+03	3.3306E+02	6.4692E+01	6.4607E+00	−6.3468E+00	−5.9917E+00	−3.5791E+00
b_6	7.8967E+03	6.1070E+02	5.8375E+01	1.4135E+01	4.8674E+00	1.1336E+00	0.2714E+00
b_7				4.7619E+01	−2.0726E+02	−2.2437E+02	6.6378E+02
b_8				−5.6325E+01	−6.4071E+01	−1.8601E+01	−9.5065E+00
b_9				−1.1098E+01	9.3634E+00	3.8169E+00	1.1208E+00
b_{10}				−1.9916E+01	−4.5169E+00	−0.3517E+00	−0.4056E−01
b_{11}					1.2613E+03	1.5070E+03	−4.9450E+03
b_{12}					−3.4412E+02	−1.9534E+02	−4.9718E+01
b_{13}					1.4623E+02	1.5579E+01	2.6483E+00
b_{14}					−8.4426E+00	−0.8457E+00	−0.1392E+00
b_{15}					1.7944E+00	0.4023E−01	0.2809E−02
b_{16}							1.6845E+04
b_{17}							−5.9670E+02
b_{18}							2.9456E+01
b_{19}							−0.4164E+00
b_{20}							0.6240E−02
b_{21}							−0.7260E−04

Table 4. Coefficients c_k for the temperature distribution in double-sine ducts with the H1 boundary condition

c_k	$\gamma = 2b/2a$						
	1/8	1/4	1/2	1.0	2.0	4.0	8.0
c_1	−0.8732E+00	−0.7512E+00	−0.5495E+00	−0.2996E+00	−0.1346E+00	−0.4734E−01	−0.1313E−01
c_2	6.5769E+00	3.0100E+00	−0.7127E−01	−0.8520E+00	−0.4890E+00	−0.1904E+00	−0.6569E−01
c_3	4.6527E+01	1.0823E+01	2.6405E+00	0.7004E+00	0.1930E+00	0.3635E−01	0.4676E−02
c_4	−1.1278E+01	2.4396E+00	3.3228E+00	−0.1799E+00	−3.9974E+00	−1.7176E+00	0.9722E−01
c_5		1.8310E+01	8.7072E+00	4.1355E+00	1.6413E+00	0.2750E+00	0.3242E−01
c_6		−2.4751E+00	−1.1314E+00	−0.4821E+00	−0.1500E+00	−0.1650E−01	−0.1140E−02
c_7				−2.1496E+01	2.7688E+01	1.2282E+01	−8.3876E+00
c_8				3.0337E+01	5.6138E+00	0.8640E+00	0.1917E+00
c_9				−9.6999E+00	−2.3628E+00	−0.1448E+00	−0.8805E−02
c_{10}				0.4172E+00	0.1080E+00	0.4499E−02	0.1634E−03
c_{11}					−1.9052E+02	−8.3398E+01	6.6259E+01
c_{12}					8.4620E+01	1.0690E+01	−0.1432E+00
c_{13}					−1.8542E+01	−0.7378E+00	−0.3787E−01
c_{14}					1.9433E+00	0.3134E−01	0.1088E−02
c_{15}					−0.4314E−01	−0.5015E−03	−0.1157E−04
c_{16}							−2.3942E+02
c_{17}							1.0289E+01
c_{18}							−0.3099E+00
c_{19}							0.4969E−02
c_{20}							−0.5127E−04
c_{21}							0.3114E−06

distribution. With $\gamma < 1$ or $\gamma > 1$, higher maximum velocities are obtained at the centerline of duct, relative to the peak velocity for $\gamma = 1$. However, as γ increases the velocity distribution tends to have an elongated profile with steeper gradients. Relatively smaller velocity gradients exist in flows through small aspect ratio cross sections ($\gamma \to 0$); in fact the flow tends to stagnate or become immovable in the corners/edges of the duct.

Temperature profiles for fully developed flows with T and H1 boundary conditions are graphed in Figs. 4 and 5, respectively. Once again, ducts with $\gamma = 0.25$, 1.0, and 4.0 are considered, and the aspect ratio is seen to have a pronounced effect on the temperature field. Reflecting the flow behavior, higher centerline-to-wall temperature differences are obtained in ducts with $\gamma > 1$ and $\gamma < 1$. Also, the profiles have sharper temperature gradients in the core of the duct in comparison

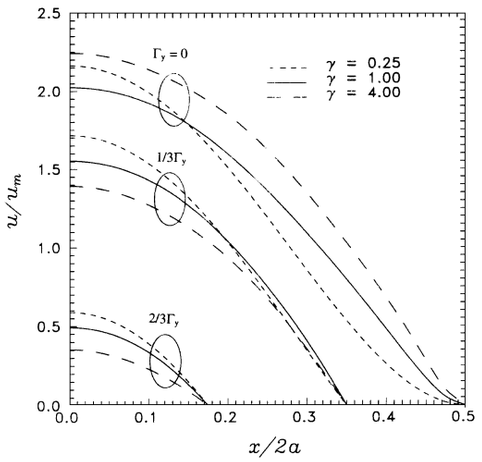

Fig. 3. Effect of aspect ratio on the velocity distribution, u/u_m, in double-sine ducts

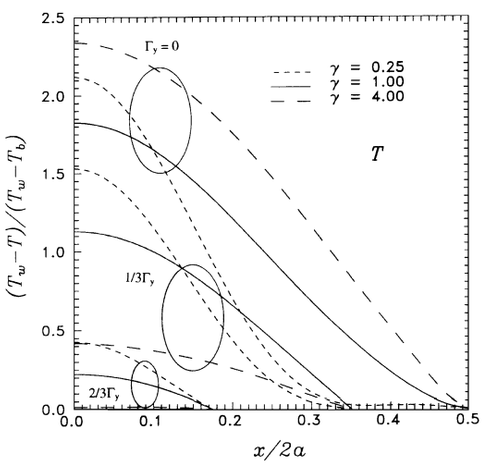

Fig. 4. Effect of aspect ratio on the temperature distribution, $(\theta/\theta_b) = (T_w - T)/(T_w - T_b)$, for the T boundary condition in double-sine ducts

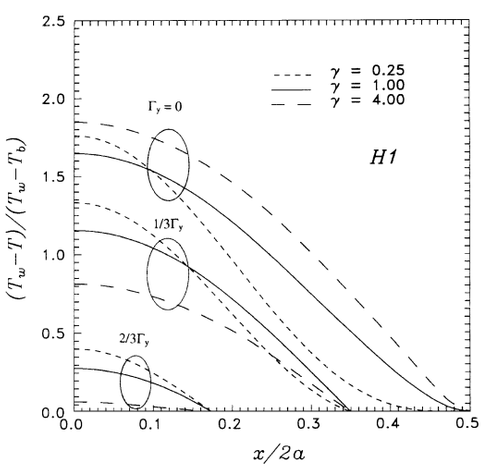

Fig. 5. Effect of aspect ratio on the temperature distribution, $(\theta/\theta_b) = (T_w - T)/(T_w - T_b)$, for the H1 boundary condition in double-sine ducts

with those near the wall. This effect is more acute with the T boundary condition; because of the constant wall temperature, the fluid near the wall attains its temperature as the flow becomes fully developed. This is clearly seen in Fig. 4, where the temperature profiles at $\Gamma_\gamma = 0$ and $1/3\Gamma_\gamma$ have a "flat" inflection in the wall region for $\gamma = 0.25$, and likewise, for $\gamma = 4.0$, the profile is virtually flat with $\Delta T \to 0$ at $2/3\Gamma_\gamma$. With the H1 boundary, on the other hand, the wall temperature "runs away" from the fluid temperature, and much sharper wall gradients are obtained. These, however, decrease with either $\gamma < 1$ or $\gamma > 1$ flow cross sections.

3.2 Friction factor and Nusselt number

Given the solutions for the isothermal velocity distribution and temperature profiles for the T and H1 boundary conditions, the respective friction factor and Nusselt number results are listed in Table 5. These are for fully developed laminar flows in double-sine shaped ducts with $1/8 \le \gamma \le 8$. As can be seen from the tabulation, *fRe* generally increases with γ, going from 14.6426 for $\gamma = 1/8$ to 17.0669 for $\gamma = 8$. This represents a change of about 16.6% in the hydraulic diameter based *fRe* over the given range of duct aspect ratio. The heat transfer performance, however, is somewhat different. Irrespective of the thermal boundary condition, as γ increases from 1/8 to 8, *Nu* increases up to $\gamma = 1.0$ and then decreases with further increase in γ. That is, the peak *Nu* is obtained for a double-sine shaped duct with an aspect ratio of unity, for both T and H1 boundary conditions. Furthermore, reflecting the appropriate effects of the respective temeperature fields, Nu_{H1} is greater than Nu_T for all cases. Depending upon γ, the ratio (Nu_{H1}/Nu_T) is seen to be between 1.2 to 1.4. Also given in Table 5 are the values for (u_{max}/u_m), $(\theta_{max}/\theta_b)_T$, and $(\theta_{max}/\theta_b)_{H1}$ for different γ. As indicated previously, the peak velocity and wall-to-fluid temperature difference increases when $\gamma < 1$ or $\gamma > 1$. This is of particular significance in process heat transfer applications, where viscous fluids that are thermally unstable are sometimes encountered. It would appear that ducts with aspect ratio close to one may be more appropriate in such usages.

Figure 6 gives a comparison of *fRe* results for double-sine shaped ducts with those for other compact channel geometries described in Fig. 1. The results for isosceles triangular, rhombic, and trapezoidal ducts are from analytical solutions reported by Shah [10]. With the exception of small aspect ratio ($\gamma < 1$) trapezoidal flow cross sections, friction factors in double-sine ducts are considerably higher than those in all other shapes considered in Fig. 6. For corrugated plate surfaces in plate heat exchangers (Fig. 2), to a first estimate these results suggest that triangular shaped corrugations (which would result in rhombic channels) would be preferable in applications with pressure drop controlled limitations.

The comparisons of Nusselt number results of various compact geometries (Fig. 1) and their variation with γ are presented in Figs. 7 and 8, respectively, for the T and H1 boundary conditions. For the T condition, along with the present solutions for sine and double-sine ducts, the analytical solutions for isosceles triangular channels [12], and numerical results for rhombic [13] and trapezoidal [8] channels are given in Fig. 7; for the H1 condition, results for the latter three geometries are from analytical solutions [10]. For the

Table 5. Fully developed laminar flow and heat transfer characteristics in double-sine shaped ducts

$\gamma=\frac{2b}{2a}$	$\frac{d_h}{2a}$	$\frac{u_{max}}{u_m}$	fRe	$\left(\frac{\theta_{max}}{\theta_b}\right)_T$	Nu_T	$\left(\frac{\theta_{max}}{\theta_b}\right)_{H_1}$	Nu_{H_1}
1/8	0.1576	2.2202	14.6426	2.3531	2.4412	1.8307	3.3418
1/4	0.3068	2.1629	14.7658	2.1225	2.7302	1.7595	3.5274
1/2	0.5585	2.0771	15.0527	1.8858	3.1676	1.6760	3.8059
1.0	0.8699	2.0250	15.5744	1.8243	3.4461	1.6462	4.1575
2.0	1.1048	2.0993	16.2861	1.9820	3.3163	1.7133	3.8840
4.0	1.2160	2.2431	16.8140	2.3372	2.9096	1.8468	3.6057
8.0	1.2557	2.3554	17.0669	2.7556	2.5492	1.9683	3.3500

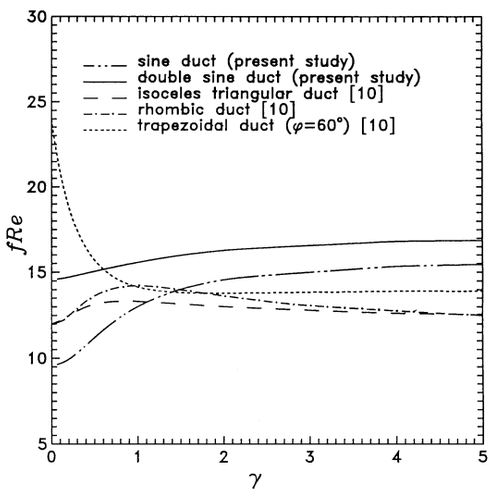

Fig. 6. Variation of fRe with aspect ratio in double-sine ducts and other compact channel geometries

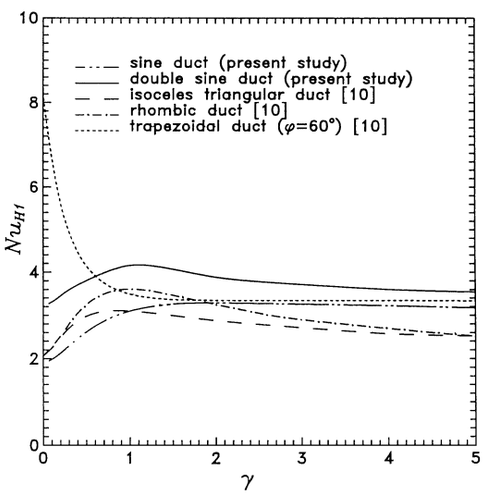

Fig. 8. Variation of Nu_{H1} with aspect ratio in double-sine ducts and other compact channel geometries

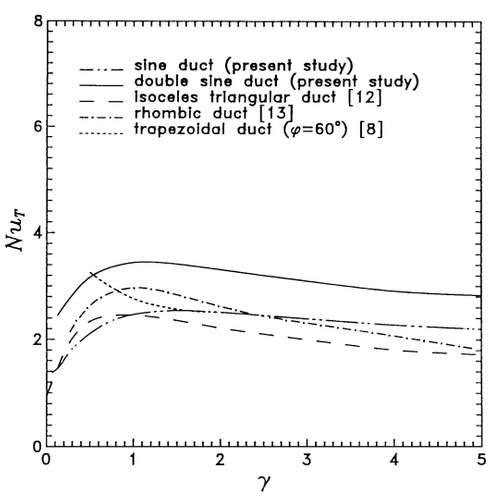

Fig. 7. Variation of Nu_T with aspect ratio in double-sine ducts and other compact channel geometries

trapezoidal cross section with T boundary condition, only limited numerical results are given by Farhanieh and Sunden [8]. Again, as in the case of fRe, the Nusselt numbers for double-sine shaped channels are much higher than those for the other geometries, for all values of γ and both T and H1 boundary conditions. The only exception is the trapezoidal shape of very small aspect ratio ($\gamma<1$). An interesting feature of these results is that the optimal (Nu/fRe) performance appears to be for $\gamma \approx 1$ for both boundary conditions. Consequently, while pressure drop constraints may warrant double-sine shapes with $\gamma<1$, the heat transfer enhancement in $\gamma \approx 1$ may, to a degree, offset this penalty.

4 Conclusions

Hydrodynamically and thermally fully developed laminar flows in double-sine shaped straight ducts have been analyzed in this paper. Very accurate, constant property solutions, for both T and H1 thermal boundary conditions, are obtained by the Galerkin function based integral method. The accuracy of the method is verified from a comparison of present solutions for sine ducts with other analytical results previously reported in the literature. From the velocity and temperature distributions, and the corresponding fRe, Nu_T, and Nu_{H1} results in double-sine ducts of varying aspect ratios ($1/8 \le \gamma \le 8$), the following observations are made:

(1) Large peak velocities and wall-to-fluid temperature differences are obtained in ducts with $\gamma<1$ or $\gamma>1$. Compared with

flows in $\gamma = 1$ channels, the velocity and temperature fields have sharper gradients in these cases.

(2) The average wall velocity gradient, and hence the friction factor increases with increasing γ (1/8→8). However, the Nusselt number decreases when $\gamma < 1$ and $\gamma > 1$ for both T and H1 conditions; the peak heat transfer performance is for $\gamma \approx 1$. Also, reflecting the thermal boundary condition effect, $Nu_{H1} > Nu_{T}$ for all γ.

(3) For plate heat exchanger applications where the plate corrugations have a sinusoidal profile and hence double-sine channels, the optimum heat transfer enhancement (nominally considered as the ratio Nu/fRe) is found to be for $\gamma \approx 1$. For usages controlled by Δp limitations, however, smaller aspect ratio ducts may be needed.

References

1. Shah, R.K.; London, A.L.: Laminar Flow Forced Convection in Ducts. New York: Academic Press 1978
2. Bergles, A.E.: Techniques to augment heat transfer. In: Handbook of Heat Transfer Applications. Rohsenow, W.M.; Hartnett, J.P.; Ganic, E.N. (Eds.), 2nd Edition, Ch. 3. New York: McGraw-Hill 1985
3. Webb, R.L.: Principles of Enchanced Heat Transfer. New York: Wiley 1994
4. Manglik, R.M.; Muley, A.: Heat transfer and pressure drop characteristics of plate-and-frame heat exchangers – a literature review. Report No. TFL-Int-1, Thermal-Fluids Laboratory, University of Cincinnati, Cincinnati, OH, September 1993
5. Shah, R.K.; Focke, W.W.: Plate heat exchangers and their design theory. In: Heat Transfer Equipment Design. Shah, R.K.; Subbarao, E.C.; Mashelkar, R.A. (Eds.), pp. 227–254. New York: Hemisphere 1988
6. Shah, R.K.; Bhatti, M.S.: Laminar convective heat transfer in ducts. In: Handbook of Single-Phase Convective Heat Transfer. Kakaç, S.; Shah, R.K.; Aung, W. (Eds.), Ch. 3. New York: Wiley 1987
7. Lakshminarayanan, R.; Haji-Sheikh, A.: Extended Graetz problems in irregular ducts. In: ASME Proceedings of the 1988 National Heat Transfer Conference. Jacobs, H.R. (Ed.), HTD-96, Vol. 1, pp. 475–482. New York: ASME 1988
8. Farhanieh, B.; Sunden, B.: Three-dimensional laminar flow and heat transfer in the entrance region of trapezoidal ducts. Int. J. Numer. Meth. Fluids 13 (1991) 537–556
9. Manglik, R.M.; Bergles, A.E.: Fully developed laminar heat transfer in circular-segment ducts with uniform wall temperature. Numer. Heat Transfer, Part A, 24 (1994) 499–519
10. Shah, R.K.: Laminar flow forced convection heat transfer in ducts of arbitrary geometry. Int. J. Heat Mass Transfer 18 (1975) 849–862
11. Schmidt, F.W.; Newell, M.E.: Heat transfer in fully developed laminar flow through rectangular and isosceles triangular ducts. Int. J. Heat Mass Transfer 10 (1967) 1121–1123
12. Haji-Sheikh, A.; Mashena, M.; Haji-Sheikh, M.J.: Heat transfer coefficient in ducts with constant wall temperature. J. Heat Transfer 105 (1983) 878–883
13. Asako, Y.; Faghri, M.: Three-dimensional laminar heat transfer and fluid flow characteristics in the entrance region of a rhombic duct. J. Heat Transfer 110 (1988) 855–861
14. Sherony, D.F.; Solbrig, C.W.: Analytical investigation of heat or mass transfer and friction factors in a corrugated duct heat or mass exchanger. Int. J. Heat Mass Transfer 13 (1970) 145–159
15. Kantorovich, L.V.; Krylov, V.I.: Approximate Methods of Higher analysis. New York: Interscience 1964
16. Cotta, R.M.: Integral Transforms in Computational Heat and Fluid Flow. Boca Raton: CRC Press 1993
17. Lakshminarayanan, R.: Integral solutions for laminar entrance problems in irregular ducts. Ph.D. Dissertation, University of Texas, Arlington, TX, 1988
18. Beck, J.V.; Cole, K.D.; Haji-Sheikh, A.; Litkouhi, B.: Heat Conduction using Green's Functions. London: Hemisphere 1992
19. Payne, F.R.; Corduneanu, C.C.; Haji-Sheikh, A.; Huang, T.: Integral Methods in Science and Engineering. Washington: Hemisphere 1986
20. Borse, G.J.: FORTRAN 77 and Numerical Methods for Engineers. Boston: PWS Publishers 1985
21. Ding, J.: Integral solutions for laminar fully developed non-Newtonian flows in irregular ducts. M.S. thesis, University of Cincinnati, Cincinnati, OH, 1995